Interplay between spin-orbit coupling and strong correlation effects: Comparison of the three osmate double perovskites Ba_2AOsO_6 (A = Na, Ca, Y)

Shruba Gangopadhyay and Warren E. Pickett
Department of Physics, University of California, Davis, California 95616, USA
(Received 28 September 2015; revised manuscript received 7 March 2016; published 15 April 2016)

High formal valence Os-based double perovskites are a focus of current interest because they display strong interplay of large spin-orbit coupling and strong electronic correlation. Here we present the electronic and magnetic characteristics of a sequence of three cubic Os based double perovskites Ba_2AOsO_6 (A = Na, Ca, Y), with formal valences of $Os^{+7}(d^1)$, $Os^{+6}(d^2)$, and $Os^{+5}(d^3)$. For these first principles based calculations we apply an "exact exchange for correlated electrons" functional, with exact exchange applied in a hybrid fashion solely to the Os ($5d$) states. While Ba_2NaOsO_6 is a reported ferromagnetic Dirac-Mott insulator studied previously, the other two show antiferromagnetic ordering while all retain the undistorted cubic structure. For comparison purposes we have investigated only the ferromagnetic ordered phase. A metal-insulator transition is predicted to occur upon rotating the direction of magnetization in all three materials, reflecting the central role of spin-orbit coupling in these small gap osmates. Surprises arising from comparing formal charge states with the radial charge densities are discussed. Chemical shielding factors and orbital susceptibilities are provided for comparison with future nuclear magnetic resonance data.

DOI: 10.1103/PhysRevB.93.155126

I. INTRODUCTION

Strong spin-orbit coupling (SOC) is a relativistic effect that couples the orbital angular momentum to the electron spin in atoms, and can often be treated as a small perturbation in the discussion of electrons in solids. However, in heavy elements SOC is not weak, and indeed can lead to striking qualitative effects. Recent interest is largely in the diverse properties of electronic materials that are insulating, or in the process of becoming so, as a result of electron-electron interactions, the most prominent one being the strong local Hubbard repulsion U between electrons within an open subshell. For these heavy ions SOC may become a competing or even dominating factor, mixing the various spin, orbital, charge, and lattice degrees of freedom.

The interplay of strong electron correlation and large SOC is relatively less explored, and certainly not well understood at all, because the behavior involves so many comparable energy scales. This situation arises in a broad family of magnetic Mott insulating systems in which threefold degenerate t_{2g} orbitals are partially filled [1]. In such systems orbital degeneracy is protected only by cubic lattice symmetry, and typically the crystal field splitting is large enough that e_g orbitals are out of the picture. Insulating states sometimes arise due to spin-orbit coupling, as shown earlier [2] for Ba_2NaOsO_6. This importance of SOC classified BNOO as a Dirac-Mott insulator [3], i.e., the combination of relativistic effects and strong repulsion is responsible for the insulating behavior.

Upon descending the Periodic Table from the $3d$ to $4d$ to the $5d$ series, there are several competing trends. First, the d orbitals become more extended, tending to reduce the electronic repulsion U and thereby diminish correlation effects. However, simultaneously, the SOC increases by an order of magnitude from $3d$ to $5d$, leading to enhanced splittings between otherwise degenerate or nearly degenerate orbitals and bands, reducing in many cases the kinetic energy as well. Bandwidths typically remain small, with overlap of the larger orbitals compensated by increase in the interatomic distances.

In $5d$ t_{2g} subshells where SOC remains unquenched (cubic symmetry), the six one-electron levels split into an upper $J = \frac{1}{2}$ doublet and a lower $J = \frac{3}{2}$ quartet. In this category Ir-based based magnets have been studied actively [4–8]. A prominent class of such systems is the ordered double perovskites (DP), with chemical formula $T_2AA'O_6$, where T is a closed shell cation. The structure is illustrated in Fig. 1. We are interested in the case where A is a closed shell cation and A' is a magnetic ion; in such cases unusually high formal valence states can arise. A few examples attracting recent interest are $A' = Ru^{5+}$ and Os^{5+} in $T_2NaA'O_6$ (T = La and Nd) [9–11], Mo^{5+} in Ba_2YMoO_6, Os^{6+} in Ba_2CaOsO_6 [12], and heptavalent Os in Ba_2AOsO_6 (A = Li, Na). For further study we have chosen three cubic Os based DPs Ba_2NaOsO_6 (BNOO), Ba_2CaOsO_6 (BCOO), and Ba_2YOsO_6 (BYOO), where the Os formal charge states vary across +7, +6, +5 with d^1, d^2, and d^3 formal configurations. Experimental work on the Ca and Y analogs of BNOO show, as does BNOO, significant decrease of their magnetic moments from their spin only values compared to their $4d$ sister compounds. Probing this question is one focus of this paper.

High formal valence has itself attracted attention for some time. How can electrons be so fickle as to leave such highly charged ions? A more specific question is the following: do such states inhibit orbital moments and thus orbital physics? High valent osmates can have an open e_g shell rather than t_{2g} shell, and e_g states nominally provide no orbital moment. Song *et al.* [13] have reported a theoretical study [13] of $KOsO_4$ with heptavalent Os in tetrahedral coordination, where large SOC, strong correlations, and structural symmetry breaking conspire to produce an unexpectedly large orbital moment in the e_g^1 shell. The moment arises due to distortion from ideal tetrahedral symmetry of the ion and modest crystal field splitting, which allows mixing in of orbitals that support an orbital moment. The high-spin d^3 configuration expected of BYOO likewise nominally provides no orbital moment, since it is a closed subshell. The chosen sequence allows an assessment of this possibility in an octahedral environment.

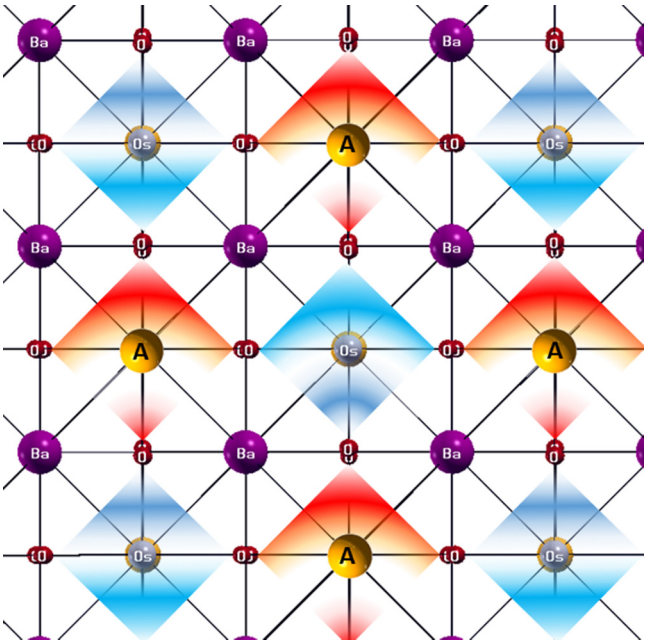

FIG. 1. Two dimensional schematic representation of face centered cubic double perovskites with a general formula Ba_2AOsO_6; blue and red shaded octahedra represent cross sections of Os-O and A-O octahedra, respectively (A = Na, Ca, Y). For these osmates the A cation is closed shell and nonbonding, leaving each Os on with its own OsO_6 cluster.

The experimental studies of these compounds [14,15] show many features to make them of current interest. Besides their undistorted cubic DP structure, and providing a sequence of heptavalent, hexavalent, and pentavalent osmium compounds, BNOO is exotic in being characterized as a ferromagnetic Mott insulator [15,16], with order appearing at $T_C = 6.8$ K with Curie-Weiss temperature $\Theta_{CW} = -10$ K. In BCOO, Curie-Weiss behavior is observed for $T > 100$ K with $\Theta_{CW} = 156$ K. BCOO did not show any ordered moment in powdered neutron diffraction [17]; however, muon spin relaxation (μSR) data indicate that long-range magnetic order develops below $T_C = 50$ K. An estimate of the ordered moment on Os^{+6} is around $0.2\mu_B$, based upon a comparison with μSR data for Ba_2YRuO_6 with its known ordered moment of $2.2\mu_B$. This moment is dramatically smaller than the spin-only value for a $5d^2$ $S = 1$ Os^{+6} configuration, implicating a major influence of SOC. BYOO exhibits a remarkably large Curie-Weiss temperature $\Theta_{CW} = 772$ K indicating strong antiferromagnetic correlations within an fcc sublattice with its high degree of magnetic frustration [18]. A magnetic transition to long range antiferromagnetic order, consistent with fcc type I order, occurs at $T_N = 69$ K. Yet again in this sequence of compounds, the Os ordered moment of $1.65\mu_B$ is much lower than the spin-only value of $3\mu_B$. A reduction of moment is unexpected in a high spin d^3 ion for which there should be no orbital moment to compensate.

Although BNOO's single t_{2g} moment orders, the structure shows no evidence of the Jahn-Teller distortion that would accompany ordering of noncubic charge density that would destroy its cubic symmetry. The sister compound La_2NaOsO_6, on the other hand, with high-spin d^3 Os configuration and a nominally cubic symmetry, is observed to be highly distorted [19]. This distortion can be understood in terms of geometrical misfit arising from incompatible ionic radii. There is another recent example of an Os-based $5d^4$ perovskite compound $BaOsO_3$ that remains cubic [20]; on the other hand, a related perovskite $5d^5$ $NaOsO_3$ does distort [21]. Again, this distortion may be due to differences in Goldschmidt's tolerance factor.

Lee and Pickett demonstrated [22] in BNOO that, before considering magnetism and on-site interaction effects, large SOC splits the t_{2g} bands into a lower $J = \frac{3}{2}$ quartet and an upper $J = \frac{1}{2}$ doublet. Since BNOO is observed to be insulating and effects of spin-orbit coupling drive the behavior, it provided the first "$J_{\rm eff} = \frac{3}{2}$" Mott insulator at quarter-filling, analogous to the "$J_{\rm eff} = \frac{1}{2}$" Mott insulators at half-filling that are being studied in $5d^5$ systems [7,23,24]. Since SOC is necessary to obtain the correct insulating ground state, these Dirac-Mott insulator states provide a descriptive distinction to conventional $3d$ Mott insulators.

Including spin polarization and on-site Hubbard U repulsion beyond the semilocal density functional approximation (DFT) within the DFT+U scheme [25–27] and including SOC in two all-electron codes, essentially full spin polarization was obtained but a gap was not opened [22] with a reasonable value of U. The basic complication seemed to be that the occupied orbital in the OsO_6 cluster has only half of its charge on Os, with the other half spread over the neighboring O ions. Thinking in terms of hybridized local orbitals (viz. Wannier functions) U should be a value appropriate to the cluster orbital and should be applied to that orbital; however, existing codes apply U only to the Os $5d$ orbitals. Xiang and Whangbo [28] neglected the Hund's rule J_H in their DFT+U calculation and did obtain a gap. However, neglecting J_H omits both the Hund's rule exchange energy and the anisotropy (orbital dependence) of the Hubbard interaction $U_{mm'}$, whereas a full treatment should include all orbital dependencies to understand the anisotropy on the Os site. Here the subscript indices m,m' denote the z projections of the atomic angular momentum.

In Sec. II the theoretical methods for this work are described. We have used an orbital-dependent hybrid DFT approach, but distinct from DFT+U methods in being parameter-free, and different from conventional hybrid methods as well. This EECE functional (see Sec. II) gave a consistent explanation [2] for BNOO of experimental observations [15] of (i) the Dirac-Mott-insulating state, (ii) the [110] easy axis, (iii) effective moment, and (iv) the retention of the cubic structure. Here we apply this method to the other two cubic Os-based DPs (BCOO and BYOO), having d^2 and d^3 Os ions, respectively, to provide a systematic comparison and contrast in this sequence of compounds.

In Sec. III we outline the theory behind the nuclear magnetic resonance (NMR) quantities that we report, in anticipation of such experiments. Results for band gaps and spin and orbital moments for three different directions of magnetization are presented and discussed in Sec. IV. A radial $5d$ charge density analysis shows another revealing feature: though the formal charge of Os in these perovskites ranges from +7 to +5, the radial charge densities on the Os ions are virtually

indistinguishable, i.e., the Os ions have the same physical 5*d* charge. This result is an extension of recent findings in other transition metal oxides [29–31]. The dependence of the NMR chemical shielding factor and susceptibility on the direction of spin is also presented. Interpretation of NMR data in heavy *d* oxides is still in an early stage. One theoretical study of magnetic susceptibility and chemical shielding parameters for the 4*d* system Sr_2RuO_4 has published, along with formal details [32]. A summary of our results is provided in Sec. V.

II. COMPUTATIONAL METHODS

The present DFT-based electronic structure calculations were performed using the full-potential augmented plane wave plus local orbital method as implemented in the WIEN2K code [33]. The structural parameters of BNOO, BCOO, and BYOO with full cubic symmetry of the DP structure were taken from experimental x-ray crystallographic data [12,16,18]: $a = 8.28$ Å, $x_O = 0.2256$; $a = 8.34$ Å, $x_O = 0.2410$; $a = 8.35$ Å, $x_O = 0.2350$, respectively. Note that the replacement Ca→Y does not change the lattice constant noticeably, but displaces the O ion somewhat. Atomic sphere radii, in a.u., were chosen as 2.50 (Ba), 2.00 (Na, Ca, Y), 1.80 (Os), and 1.58 (O). The Brillouin zone was sampled with a minimum of 400 *k* points during self-consistency, since coarser meshes were sometimes found to be insufficient.

A. On-site exact exchange: EECE functional

For the exchange-correlation energy functional for treating strongly correlated insulators, a variety of approaches in addition to DFT+*U* exist and have been tested and compared for a few selected systems [34]. In the *philosophy* behind the DFT+*U* approach, the relevant orbital is accepted to be, not an atomic orbital, but rather that orbital hybridized with neighboring ligand orbitals, or (almost) equivalently, a Wannier orbital. In the systems we treat this would be an OsO_6 octahedron cluster orbital. However, codes that implement the DFT+*U* method use an atomic orbital (or most of one, lying within an atomic sphere), and apply the exchange energy shift *U* and Hund's exchange shift J_H to this orbital.

However, the physical process that is not represented well in semilocal DFT is the *exchange interaction on the transition metal ion* (here Os). More direct treatment of exchange has been addressed with hybrid methods, which use for the exchange functional a fraction of local density exchange and another fraction (the complement of unity) of bare Hartree-Fock exchange. Not only is this conventional hybrid approach computationally expensive, it treats (and approximates) exchange interactions between itinerant states that may just as well be treated by efficient semilocal methods.

For this study we have chosen to apply the "exact exchange for correlated electrons" (EECE) functional for treating correlated electron systems, introduced and evaluated by Novak and collaborators [35]. Exact (Hartree-Fock) exchange is applied only to the correlated orbitals (5*d* for osmium) with full anisotropy of the exchange, and then implemented similarly to common use in hybrid functionals, with 25% of local density exchange being replaced by exact on-site exchange. Although this EECE functional has not been applied widely for Mott insulators, it has been found that it reproduces features of the DFT+*U* method—opening of a gap in open-shell *d* systems, for example—without reference to any screened Hubbard *U* and Hund's rule J_H parameters, and without facing the choice of the type of double-counting correction [27] to choose. As noted in the Introduction, the EECE functional treatment makes the unusual Dirac-Mott insulating ferromagnetic ground state of BNOO fully comprehensible. We note that in a previous publication a different acronym was used for this method [2], but here we return to the original use of EECE.

We use this functional as implemented in the WIEN2K code [36], version 14.2. For the semilocal exchange-correlation part of the functional, the parametrization of Perdew, Burke, and Ernzerhof [37] [generalized gradient approximation (GGA)] is used. SOC was included fully in core states and for valence states was included in an accurate second-variational method using scalar relativistic wave functions [38], a procedure that is nonperturbative and quite accurate for *d* orbitals even with large SOC.

This EECE method bears some kinship with the more conventional hybrid exchange-correlation functionals (see Tran *et al.* [34] for a comparison of several hybrid functionals). Hybrids replace some fraction, typically 25%, of local density exchange with Hartree-Fock exchange, which often is approximated in various ways to reduce the expense to a more reasonable level. The EECE approach deals with exact exchange only for correlated orbitals, however, making it appropriate for correlated materials. Note that it does not increase band gaps of ionic or covalent semiconductors, being more appropriate for local orbital systems.

III. NMR RELATED QUANTITIES

A. Calculation of chemical shielding

The chemical shift calculations are based on an all-electron linear response method where one obtains the induced current density considering the perturbation of the ground state wave functions due to the external magnetic field. The resulting magnetic shielding is then obtained by integration of the all-electron current according to the Biot-Savart law without further approximations.

Here, we outline the method of calculation of the NMR shielding. The approach is based on a linear response theory widely used for the NMR properties of solids [39–42]. A detailed description of implementation of this approach into WIEN2K [39–41] was provided recently [41,42], and we summarize this approach here.

The chemical shielding tensor $\overleftrightarrow{\sigma}$ is a proportionality factor (a linear response coefficient) between the induced magnetic field $\boldsymbol{B}_{\mathbf{ind}}$ measured at the nucleus at site $\mathbf{R}$ and the external field $\mathbf{B}$:

$$\mathbf{B}_{\mathrm{ind}}(\mathbf{R}) = -\overleftrightarrow{\sigma}(\mathbf{R})\mathbf{B}. \tag{1}$$

For the materials we study, we deal with the isotropic shielding (IS), which is given by $\sigma(\mathbf{R}) = \mathrm{Tr}[\overleftrightarrow{\sigma}(\mathbf{R})]$. The experimentally measured chemical shift δ of the resonance line is expressed with respect to some reference, so $\delta(\mathbf{R}) = \sigma_{\mathrm{ref}} - \sigma(\mathbf{R})$. The induced field $\mathbf{B}_{\mathrm{ind}}$ is evaluated by integrating

the induced current $\mathbf{j}_{\rm ind}(\mathbf{r})$ according to the Biot-Savart law:

$$\mathbf{B}_{\rm ind}(\mathbf{R}) = -\frac{1}{c}\int d^3r\, \mathbf{j}_{\rm ind}(\mathbf{r})\frac{\mathbf{r}-\mathbf{R}}{|\mathbf{r}-\mathbf{R}|^3}. \quad (2)$$

The calculations presented in this work have been performed using the WIEN2K [39] implementation and are based on the augmented plane wave plus local orbital (APW+lo) method with the EECE [35] exchange correlation functional. Within this method, the unperturbed wave functions as well as their first-order perturbations providing $\vec{j}_{\rm ind}$ are expressed using plane waves in the interstitial region and an atomiclike representation inside the atomic spheres. In contrast to standard ground-state calculations, evaluation of the isotropic shielding requires an extended basis set inside the spheres, which is achieved by supplying additional local orbitals as described by Laskowski and Blaha [39]. To ensure convergence, we use ten extra local orbitals for Ba, the A atom (Na, Ca, Y), Os, and O. For other computational parameters, the standard values for electronic structure studies lead to well-converged results. k point sampling of the Brillouin zone was done with a $7\times7\times7$ mesh in these insulating (or nearly insulating) states.

B. Macroscopic magnetic susceptibility

Application of a uniform magnetic field results in both spin and orbital magnetic responses, described by the respective susceptibilities. The orbital magnetic susceptibility χ determines the macroscopic component of the induced orbital magnetic field, which may result in a contribution of several ppm to the chemical shielding. To obtain the macroscopic susceptibility $\overleftrightarrow{\chi}$ that enters $\mathbf{B}_{\rm ind}(\mathbf{G}=0)$, the method follows Mauri and Pickard [43], using

$$\overleftrightarrow{\chi} = \lim_{q\to0}\frac{\overleftrightarrow{F}(q) - 2\overleftrightarrow{F}(0) + \overleftrightarrow{F}(-q)}{q^2}, \quad (3)$$

where $F_{i,j} = (2-\delta_{i,j})Q_{i,j}$ and i and j are Cartesian indices. The tensor $\overleftrightarrow{Q}$ is given by

$$\overleftrightarrow{Q}(q) = \Omega_c \sum_{\alpha=x,y,z}\sum_{o,\mathbf{k}} \mathrm{Re}\left[\mathbf{A}^o_{\mathbf{k},q_\alpha}\left(\mathbf{A}^o_{\mathbf{k},q_\alpha}\right)^*\right], \quad (4)$$

where $\mathbf{A}^o_{\mathbf{k},q_\alpha}$ are the momentum matrix elements between Bloch states at $\mathbf{k}$ and $\mathbf{k}+\mathbf{q}_\alpha$,

$$\mathbf{A}^o_{\mathbf{k},\mathbf{q}_\alpha} = \hat{\alpha}\times\langle u_{o,\mathbf{k}}|(\mathbf{p}+\mathbf{k})|u^{(1)}_{\mathbf{k}+\mathbf{q}_\alpha}\rangle, \quad (5)$$

these being the matrix elements occurring in the expression for the current density. α is the Cartesian direction and $u^{(1)}_{\mathbf{k}+\mathbf{q}_\alpha}$ is the periodic part of the perturbed wave function.

IV. ELECTRONIC AND MAGNETIC CHARACTERISTICS

An understanding of the effects of several competing energy scales in $5d$ oxides, viz. bandwidth, repulsive interaction energy U, SOC strength, and magnetic exchange splitting, which in these systems are all of the order of 0.5–1.5 eV, is only recently being pursued in some detail. For this reason we provide several results on this series of DPs to contribute to the building of understanding.

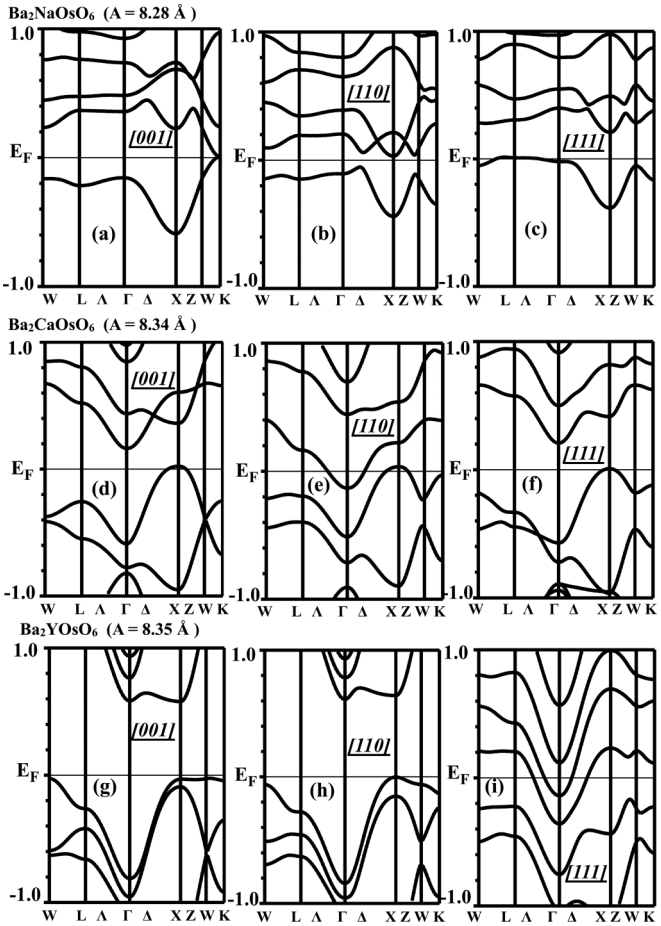

FIG. 2. Comparison band plots for Ba_2NaOsO_6 (a)–(c), Ba_2CaOsO_6 (d)–(f), and Ba_2YOsO_6 (g)–(i) for the three directions of magnetization axis (indicated on the plots), showing how the band structure depends on the direction of magnetization. Spin-orbit coupling including spin-exchange splitting leads to several distinct W, X, and K points in the zone. The symmetry points chosen for presentation are, in units of $\frac{2\pi}{a}$: W = $(1,\frac{1}{2},0)$, L = $(\frac{1}{2},-\frac{1}{2},-\frac{1}{2})$, Γ = (0,0,0), X = (1,0,0), W = $(1,\frac{1}{2},0)$, and K = $(\frac{3}{4},\frac{3}{4},0)$.

A. Band dependence on spin direction

It was shown previously that the band structure of BNOO shows strong dependence on the direction of the spin, reflecting the strong SOC. The gap is small, and an insulator-metal transition (band overlap) occurs as the direction of spin is rotated. We compare with the corresponding behavior for BCOO and BYOO in Fig. 2. We use experimental structures and ferromagnetic order to allow the most direct comparison, and the progression with band filling in this series.

Table I presents various contributions to the magnetism and the value of the calculated gap. The results are consistent with expectations in most cases; orbital moments are smaller for the filled subshell d^3 case, although by only a factor of 2–3 indicating some mixing of e_g states. The spin moment is closely proportional to the band filling, as expected for a fully polarized ion. In all cases, the spin moment is reduced when SOC is included, by 5%–15%, and hardly depends on the direction of spin. The same is true of the orbital moment,

TABLE I. Calculated spin, orbital, and total ($\mu_{\rm tot} = \mu_s + \mu_\ell$) moments ($\mu_B$) in the Os *sphere*, the spin moments on the O sites, and the band gap (eV) of Ba_2AOsO_6 (A = Na, Ca, Y). Values are presented for the three spin directions. The non-negligible interstitial contribution to the spin moment means that "Os" and "O" contributions are somewhat dependent on the choice of sphere radii.

Method	μ_s^{Os}	$\mu_{\rm orb}^{Os}$	μ_s^A	$\mu_{\rm tot}^{Os}$	$\mu_s^{O_{x/y}}$	$\mu_s O_z$	Band gap (eV)
Ba_2NaOsO_6 $\mu_{\rm interstitial} = 0.1$							
EECE	0.59	N/A	0.0001	N/A	0.02		No gap
EECE+SOC (001)	0.52	−0.41	0.0001	0.11	0.01	0.03	0.02
EECE+SOC (110)	0.52	−0.44	0.0001	0.08	0.01	0.01	0.28
EECE+SOC (111)	0.52	−0.45	0.0001	0.07	0.02	0.02	0.30
Ba_2CaOsO_6 $\mu_{\rm interstitial} = 0.3$							
EECE	1.32	N/A	0.002	N/A	0.08		No gap
EECE+SOC (001)	1.14	−0.61	0.002	0.53	0.09	0.04	0.13
EECE+SOC (110)	1.17	−0.24	0.002	0.93	0.08	0.04	No gap
EECE+SOC (111)	1.15	−0.52	0.002	0.63	0.08	0.08	0.28
Ba_2YOsO_6 $\mu_{\rm interstitial} = 0.6$							
EECE	1.8	N/A	0.02	N/A	0.09		No gap
EECE+SOC (001)	1.73	−0.16	−0.02	1.57	0.09	0.09	0.58
EECE+SOC (110)	1.72	−0.11	0.01	1.61	0.09	0.09	0.66
EECE+SOC (111)	1.74	−0.13	0.02	1.61	0.09	0.09	No gap

with one exception: for d^2 BCOO the orbital moment is much smaller for spin along [110] than for the other two directions.

The occurrence, and value, of the gap is dependent on direction of spin (Table I), due to change of symmetry and thereby of orbital occupation, as found earlier for BNOO [2]. A relevant part of the band structures are shown in Fig. 2, for this series of compounds—i.e., the t_{2g} band filling—and each of the [001], [110], and [111] spin directions. The behavior is complex and not always intuitive. The high spin d^3 configuration might be expected to be a simple band insulator, but it is so for only two directions of spin. For spin along [111], BYOO defies Dirac-Mott tendencies and retains a strongly metallic character. Thus SOC can thwart insulating character as well as encourage it, depending on other factors. In all other panels, a topological distinction between valence and conduction bands is evident, even if there is band touching or indirect overlap.

To be more explicit about the effects of symmetry lowering on the band structure by SOC, Fig. 3 displays the bands for three different Γ-W-K-Γ excursions for spin along [001] in BCOO, similar to that shown previously for BNOO. Though the gap persists at a similar value along these lines, the linear band behavior at the K point is very much different for the top valence band near the right side of this figure, with interaction with the next lower band being diminished.

B. Magnetocrystalline anisotropy

BNOO has its reported experimental easy axis along the [110] direction. Our earlier calculations [2] successfully reproduced that result; however, the energy for [111] is very close to that of [110]. The [001] spin direction lies higher in energy. For ferromagnetic alignment, BCOO and BYOO both have a [001] easy axis. The spin density of BCOO is pictured in Fig. 4. The energy differences are material dependent, in the 1–10 meV range. One feature in common for these three materials is that a metallic band structure correlates with a higher energy, i.e., metallic phases are always disfavored. This result is consistent with the observed insulating behavior observed in this series of compounds, and may result from extra kinetic energy of the conduction bands.

It can be observed that the direction of largest orbital moment does not always correspond to the easy axis. For weak SOC, there is reason to connect the direction of easy axis with largest orbital moment, since the gain in energy is presumed to arise from adjustment of the orbital moment. For large SOC, other tendencies compete. Most importantly, probably, is that the spin (hence orbital) direction influences the orbital occupation substantially. Orbital reoccupation affects many components of the energy: kinetic, Hartree, exchange, and correlation, with much compensation (since the anisotropy energies are small). This complex behavior is connected with

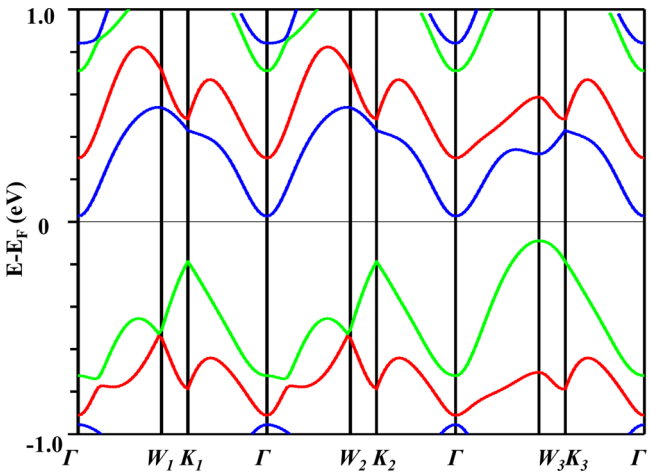

FIG. 3. Band plot along three Γ-W-K-Γ directions for Ba_2CaOsO_6 with [001] magnetization axis (a = 8.35 Å), illustrating the large effect (up to 200 meV) of symmetry lowering by the large spin-orbit interaction strength. The chosen points, in units of $\frac{2\pi}{a}$, are Γ = (0,0,0), $W_1 = (-\frac{1}{2},0,1)$, $W_2 = (0,-1,\frac{1}{2})$, $W_3 = (1,0,-\frac{1}{2})$, $K_1 = (-\frac{3}{4},0,\frac{3}{4})$, $K_2 = (0,-\frac{3}{4},\frac{3}{4})$, and $K_3 = (\frac{3}{4},0,-\frac{3}{4})$.

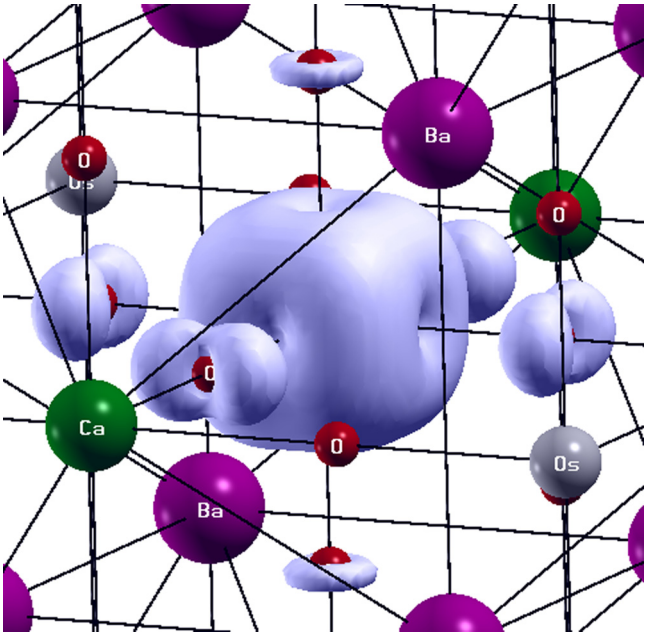

FIG. 4. Isosurface plot of the spin density (equal to the valence charge density) of d^2 BCOO for [001] spin orientation. The near-cubic shape of the density on the Os ion supports the lack of any discernible Jahn-Teller distortion from cubic symmetry. There is more induced spin density on the equatorial O ions than on the apical ions. This plot was generated by XCRYSDEN [44].

the several similar energy scales: bandwidth, on-site repulsion, Hund's exchange, crystal field splitting, and SOC.

C. SOC and spin-orbital occupations

To further illuminate the effects of SOC and spin direction in a 5*d* perovskite in a 5*d* DP, we tabulate in Table II the 5*d* spin-orbital occupations for d^2 BCOO for the three different spin directions. BCOO is chosen because it has the largest orbital moments. Several noteworthy results can be discerned from Table II. First, though Os in BCOO is nominally fully spin-polarized d^2, the spin-orbital occupations indicate complexity behind this formal charge designation. The total 5*d* occupation number sum is around 3.4, not 2.0. Moreover, much of the 5*d* charge lies outside the sphere used to define these occupations. The largest spin-orbital occupation in the table is 0.7; this value should be understood as "full occupation." Thus the actual 5*d* charge is in the 4.5–5 electron range, versus the formal value of 2. This difference reflects the fact that formal charge is often substantially different from real charge. This distinction between charge occupation (which is difficult to identify objectively) and (integer) formal charge is reasonably well recognized by electronic structure practitioners, and the distinction is important to take into account if one tries to understand the spin-orbital occupations. We return to the actual 5*d* charge issue in Sec. IV E.

TABLE II. 5*d* orbital specific occupation for Ba_2CaOsO_6, using three spin directions [001], [110], and [111]. Spin up and spin down orbital occupations along with the difference (Net spin) are displayed; the meaningful ones are in boldface and appear clearly in the net spin. The total occupation sum of the *5d* shell (right hand column) remains the same for the different spin directions.

SOC direction [001]	m_l	−2	−1	0	+1	+2	Sum
Spin up		**0.56**	**0.70**	0.30	0.26	0.42	2.23
Spin down		0.21	0.21	0.27	0.23	0.26	1.19
Net spin		**0.35**	**0.49**	0.03	0.03	0.16	1.04
SOC direction [110]	m_l	−2	−1	0	+1	+2	Sum
Spin up		0.40	**0.58**	0.29	**0.58**	0.40	2.24
Spin down		0.24	0.21	0.27	0.21	0.24	1.18
Net spin		0.16	**0.37**	0.02	**0.37**	0.16	1.06
SOC direction [111]	m_l	−2	−1	0	+1	+2	Sum
Spin up		**0.61**	0.31	**0.69**	0.39	0.25	2.24
Spin down		0.21	0.24	0.20	0.27	0.26	1.18
Net spin		**0.40**	0.07	**0.49**	0.12	−0.01	1.06

Table II reveals, most broadly, that the net spin moment, and in fact its majority and minority contributions, are independent of spin direction, in line with the simplest picture of effects of SOC. Comparing the m_l specific 5*d* occupation numbers, one notices that spin down occupations hardly change; there is 5*d* minority spin occupation but in the net moment it remains out of the picture. The majority spin occupations do vary with spin direction, but in a more involved fashion than simple ionic models would predict. The two largest majority orbital occupations are emphasized in Table II. For each spin direction, there are two primary occupations (following the formal $5d^2$ charge state), but these vary with spin direction and the largest occupations differ in size. For the various spin directions, the two "occupied orbitals" are as follows: [001], $m_l = -2, -1$; [110], $m_l = -1, +1$; [111], $m_l = -2, 0$. Only for [001] spin direction do these follow Hund's second rule. These values reflect the strong environmental effects: the localized orbitals are not simple Os 5*d* orbitals but rather are OsO_6 molecular orbitals where the orbital moment behavior becomes unpredictable without full calculation.

D. Spin and orbital moments

The EECE functional was applied previously [2] to understand observed behavior in BNOO, providing a description of the ferromagnetic Mott insulating ground state, the [110] easy axis, and the lack of Jahn-Teller distortion which leaves BNOO with the undistorted cubic structure. Although BCOO and BYOO, unlike what is reported for BNOO, order antiferromagnetically [17,18], we make comparisons using ferromagnetic alignment of moments. The magnetic ordering question becomes very involved when SOC is large, resulting in tensor exchange coupling between mixed spin orbitals [45,46], and we do not address that question here. As in the previous work on BNOO [2], calculations are first converged without SOC, then the direction of spin is chosen and SOC is applied. Several results are presented in Table I. As mentioned above, the spin moment of Os (μ_s^{Os}) increases linearly with formal charge of Os, and μ_s^{Os} values are decreased somewhat by SOC, more so for BCOO.

The orbital moment always opposes the spin moment, in agreement with Hund's third rule. For d^1 BNOO and d^3 BYOO $\mu_{\rm orb}^{Os}$ values are almost invariant with respect to spin direction. BCOO behaves quite differently: $\mu_{\rm orb}^{Os}$ is -0.6 to $-0.5\mu_B$ for

[001] and [111] directions, but is somewhat less than half that for spin along [110]. Thus the orbital moment of Os on BCOO is larger, as expected, than on the other two materials, but also is sensitive to the direction of the spin, an unappreciated aspect of magnetocrystalline anisotropy. The contributions of the various O ions differ depending on the symmetry remaining after SOC is included.

The observed low temperature ordered moment on BYOO is $1.65\mu_B$,[18] which is much reduced from the naive spin only value of $3\mu_B$ (and no orbital contribution from the filled subshell). Table I gives the calculated Os moment *within its sphere* in BYOO of 1.57–$1.71\mu_B$, depending on the direction of spin. Our magnetocrystalline anisotropy energy calculation shows [001] is the easy axis for ferromagnetic ordered BYOO; in that case the Os effective magnetic moment is $1.57\mu_B$, naively close to the experimental value [18]. However, the net moment should be equal to the *total* spin moment minus the *total orbital* moment. The full spin moment (of the cell, i.e., of the OsO_6 cluster) is around $2.6\mu_B$, reduced by SOC from $3\mu_B$. From the orbital occupations of Table II, the largest value is 0.70, meaning that the remaining 30% lies outside the sphere, so the sphere orbital moments should be scaled up by $\frac{1}{0.7} = 1.43$. For Os in BYOO, this is about $0.2\mu_B$, making the net moment $2.4\mu_B$, still considerably larger than the observed ordered moment. The resolution to this paradox is that BYOO is actually AFM ordered, in which case the spin moment of the OsO_6 cluster may be, and most likely is, reduced from the full $3\mu_B$ value. Thus our FM moment provides no quantitative means to compare with the observed AFM value.

The question of the BNOO moment remains, as does the issue of FM order in BNOO, since the sister compounds BCOO, BYOO, and Ba_2LiOsO_6 all show AFM order. A possible resolution is that the FM order in BNOO is actually canted AFM order, in which case the basic exchange coupling is antiferromagnetic between nearest neighbors, but this is frustrated in the fcc sublattice. The balance is contained in other elements of the tensor coupling. With canted AFM order, the ordered moment is some fraction of the net local moment. Neutron scattering data might resolve these questions.

E. Radial charge density analysis

This sequence of three descending formal valence osmates provides the opportunity to address recent developments in the understanding of formal charge states [29–31]. The d^1,d^2,d^3 sequence suggests substantially differing charges on the Os ions, even if the unit difference in formal charge is not expected. Several cases have arisen recently—rare earth nickelates [29], AgO [31], and a few others [30]—where charges on differing charge states have produced perplexing results: the actual charges don't differ. Figure 5 presents the radial charge densities for the Os ion for all three double perovskites in this series. Notwithstanding the formal charges +7, +6, +5, or configurations d^1,d^2,d^3, respectively, the radial charge density in the region of the peak in 5*d* charge shows no difference, down to the subpercent level. This finding is surprising but consistent with several other examples; it is simply too costly energetically for ions to have differing physical charges. The experimental evidence for charge ordering—cation-O distances, core level differences, magnetic moments—are reproduced in calculations where there is no difference in cation charge. The formal valence concept remains an important concept, but is a property of an ion and its environment rather than of the ion alone.

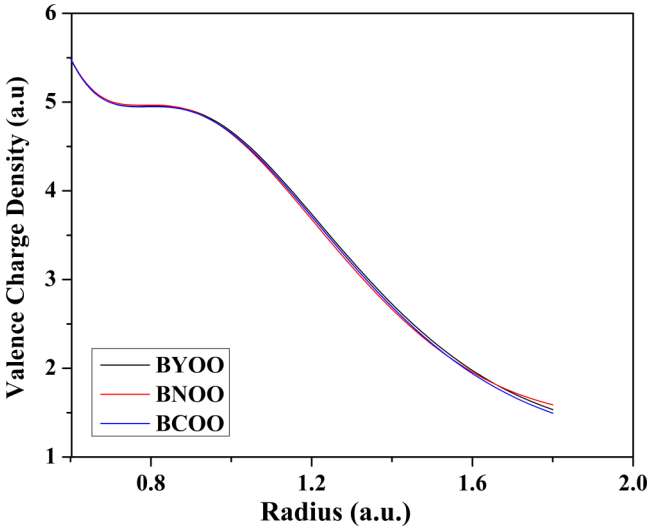

FIG. 5. Plot of the radial valence charge density on Os for the three double perovskites, restricted to the region outside the 4*f* shell. The 5*d* density peak occurs around 0.9 a.u. The three curves coincide until near the sphere boundary, where the charge is affected by tails from neighboring O ions. There is negligible difference in the 5*d* peak region, indicating no difference in 5*d* charge on Os for this sequence with formal charges of d^1,d^2, and d^3.

This constancy of 5*d* charge on Os prompted us to look at the sphere charges of the other atoms. The Ba and O atoms, which are common to this sequence of compounds, have nearly identical radial charge densities across the series (as their formal valences suggest), with roughly +3 and −1.3 net charges within the spheres used in the calculations. Note that these do not and should not closely reflect the formal charges, partly because inscribed (nonoverlapping) spheres are used, and much charge remains in the interstitial region. Na, Ca, and Y sphere charges should not be compared, as the same sphere size has been used for ions of differing charge. The differences in total charge are accommodated almost entirely in the interstitial region, possibly concentrated in the near environment of the Na, Ca, and Y ions.

F. Magnetic susceptibility and chemical shielding

There is little intuitive understanding for the types of compounds being studied here of what characteristics, and what energy ranges, of wave functions influence the macroscopic magnetic susceptibility χ and the chemical shielding fraction measured in NMR experiments. It is unclear for example if states near the band edge are particularly important, and just how large (strong) spin-orbit coupling effects are. We have evaluated these properties as described in Sec. III B. For consistency in the comparison, we have used the same muffin tin radii for Ba, Os, O for all three compounds, and for Na, Ca, Y also the same values of muffin tin radius were used.

Figure 6 shows the macroscopic orbital susceptibility χ values for the three compounds, without SOC and then

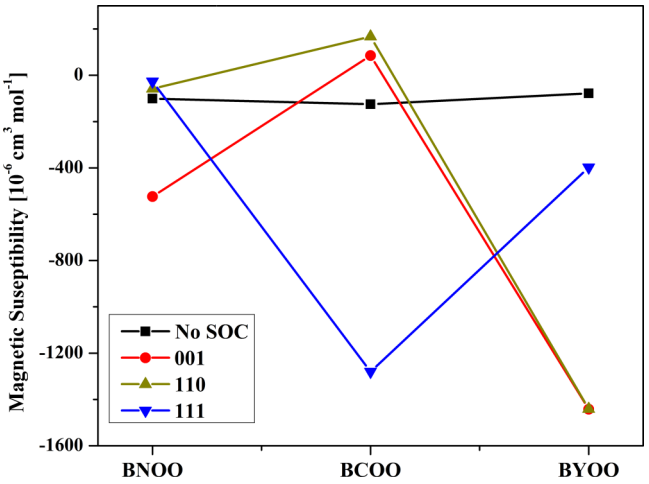

FIG. 6. Macroscopic magnetic susceptibility χ calculated for BNOO, BCOO, and BYOO, first without spin-orbit coupling, then for the three different spin directions [001], [110], and [111]. Without spin-orbit coupling χ is the same (and small) for all three. Including spin-orbit coupling results in substantial changes, nonmonotonic behavior across the series, and dependence on spin orientation.

including SOC to assess the effect. Without SOC all are predicted to have almost the same small diamagnetic value of χ. SOC results in substantial changes: some of the values become strongly diamagnetic, and the behavior is nonmonotonic with band filling. For [001] and [110] spin directions χ follows a similar trend, a positive trend from d^1 to d^2 (i.e., less negative) followed by a steep diamagnetic swing for d^3 BYOO. Another way to look at these results is that d^2 BCOO contains more paramagnetic contributions to χ than do the other two. The prediction is that the spin direction can be as important in determining χ as the band filling, and that there is no clear correlation (with spin direction, with filling, or with band gap) in this small sample. In short, SOC is the determining factor in the susceptibility of these compounds.

Figure 7(a) presents the isotropic chemical shielding parameters before inclusion of spin-orbit coupling. Except perhaps for Os, the values of σ for Ba, O, and the closed shell A cations vary little across the three compounds. The values for Na and O are very small, for Ba are positive and larger (3000 ppm). The Os value has more interesting nonmonotonic behavior, changing from large and negative for BNOO to small and positive for BCOO, then small and negative for BYOO. Evidently the polarizable $5d$ electrons in a d^1 configuration provide a better platform for induced orbital currents.

Spin-orbit coupling alters the chemical shielding fraction behavior, especially for Os. For all three directions of spin Figs. 7(b)–7(d), σ for Os becomes monotonic with formal valence and not seriously deviating from linear while staying negative. SOC makes only small changes in σ for Na and O ions, staying about the same for all three compounds. When there are two O sites due to SOC lowering of symmetry, Figs. 7(b)–7(c), there is no difference in σ. For Ba, σ increases substantially to 2500–3000 ppm and is relatively constant across the series. Experimental data will be extremely useful

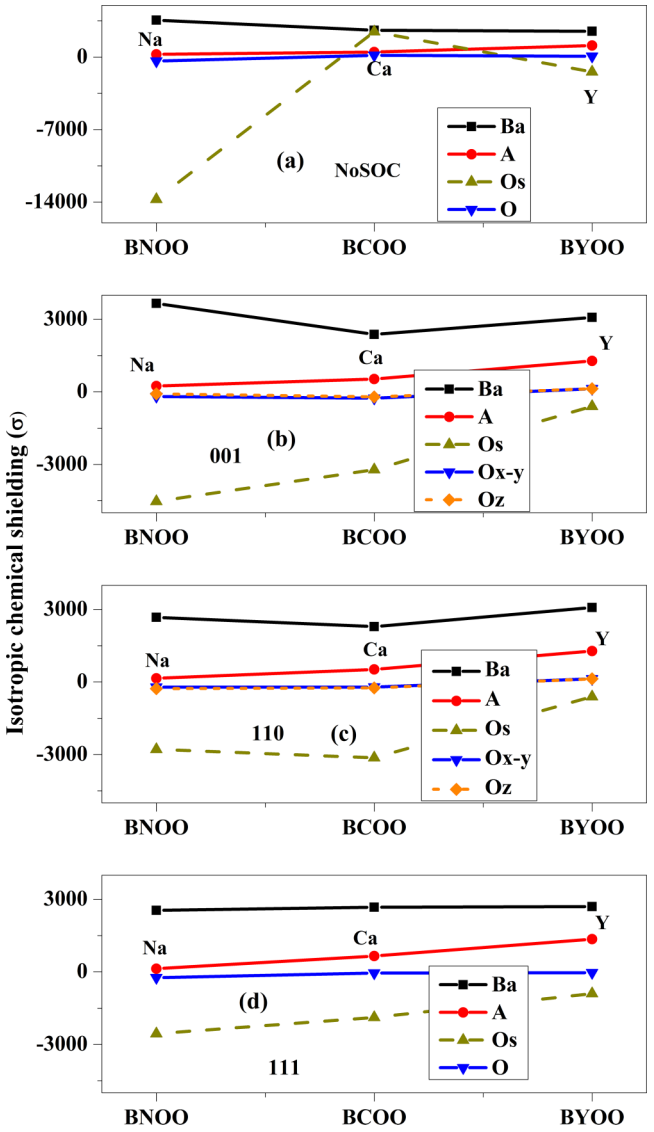

FIG. 7. Isotropic shielding fractions σ (in ppm) calculated as described in the text. Results are shown (a) without and (b)–(d) with spin-orbit coupling along three spin orientations: (b) [001], (c) [110], and (d) [111].

in understanding what can be understood and extracted from the calculated values.

Pavarini and Mazin [32] suggested that NMR related properties are mainly tuned by the orbital participation near Fermi level in the correlated metal Sr_2RuO_4 that they studied, which is known to harbor spin fluctuations. These osmates are insulating for two of the three spin directions, and the shielding fractions do not seem to be influenced much by the small metallic density (when it is present). Figure 2 indicates that bands near the gap have only significant Os $5d$ and O $2p$ character. Figure 7(a) shows that the shielding fraction on Os does not follow linear behavior versus formal d occupations before including SOC. However, when SOC is applied, Figs. 7(b)–7(d) show that monotonic (or nearly so) progression is restored. Not surprisingly, the shielding fraction on the other ions is hardly affected by SOC.

V. SUMMARY

The EECE functional, in which exact exchange in the Os 5*d* shell is combined in hybrid fashion with local density exchange elsewhere, has been used to model the sequence of increasing formal $5d^n$ osmates ($n = 1$–3) Ba_2AOsO_6, A = Na, Ca, and Y. Spin-orbit coupling is essential in opening the gap, putting all three in the "Dirac-Mott" class of correlated insulators. The gaps are predicted to be small (a few tenths of eV) and rotation of the direction of magnetization can produce an insulator-metal transition through band overlap. For insight into the spin and orbital nature of 5*d* ions, we presented an example of the effect of SOC through the *5d* orbital occupation matrix. Irrespective of spin direction the total occupation stays constant, but orbital-specific occupation depends considerably on direction of magnetization, leading to different orbital moments.

For comparison with (near) future NMR data we have presented the effect of SOC on the macroscopic susceptibility and the chemical shielding fraction. Spin-orbit coupling has a substantial effect on the susceptibility as well as the shielding fraction. Comparison of the radial charge densities reveals that the three differing formal charge states have the same physical Os 5*d* charge, a surprising result but one consistent with recent finding in 3*d* "charge ordered" systems. This result is more striking when it is realized that formal charge states differing by two (d^1 versus d^3) have the same physical charge. This result reemphasizes that formal charge is a property of an ion and its environment, which is not well recognized.

The interplay of spin-orbit coupling and correlation effects is an active area of study. Results here demonstrate that, while this interplay is substantial in 5*d* oxides, a real understanding of full outcomes must include additional aspects, such as the direction of the magnetization and its interplay with spin-orbital occupation.

ACKNOWLEDGMENTS

We acknowledge many useful conversations with K.-W. Lee and comments on the calculations from A. S. Botana. Our research used resources of the National Energy Research Scientific Computing Center (NERSC), a DOE Office of Science User Facility supported by the Office of Science of the U.S. Department of Energy under Contract No. DE-AC02-05CH11231. S.G. was supported by U.S. DOE Stockpile Stewardship Academic Alliance Program under Grant No. DE-FG03-03NA00071, and W.E.P. was supported by U.S. DOE Grant No. DE-FG02-04ER46111.

[1] G. Chen, R. Pereira, and L. Balents, Phys. Rev. B **82**, 174440 (2010).
[2] S. Gangopadhyay and W. E. Pickett, Phys. Rev. B **91**, 045133 (2015). In this paper the EECE method used in this paper was referred to as oeeHyb. In this paper and henceforward we return to the original name and acronym.
[3] H. Ishizuka and L. Balents, Phys. Rev. B **90**, 184422 (2014).
[4] G. Jackeli and G. Khaliullin, Phys. Rev. Lett. **102**, 017205 (2009).
[5] B. J. Kim, H. Jin, S. J. Moon, J.-Y. Kim, B.-G. Park, C. S. Leem, J. Yu, T. W. Noh, C. Kim, S.-J. Oh, J. H. Park, V. Durairaj, G. Cao, and E. Rotenberg, Phys. Rev. Lett. **101**, 076402 (2008).
[6] S. J. Moon, H. Jin, K. W. Kim, W. S. Choi, Y. S. Lee, J. Yu, G. Cao, A. Sumi, H. Funakubo, C. Bernhard, and T. W. Noh, Phys. Rev. Lett. **101**, 226402 (2008).
[7] B. J. Kim, H. Ohsumi, T. Komesu, S. Sakai, T. Morita, H. Takagi, and T. Arima, Science **323**, 1329 (2009).
[8] G. Cao, T. F. Qi, L. Li, J. Terzic, S. J. Yuan, L. E. DeLong, G. Murthy, and R. K. Kaul, Phys. Rev. Lett. **112**, 056402 (2014).
[9] A. A. Aczel, D. E. Bugaris, J. Yeon, C. de la Cruz, H.-C. zurLoye, and S. E. Nagler, Phys. Rev. B **88**, 014413 (2013).
[10] A. A. Aczel, P. J. Baker, D. E. Bugaris, J. Yeon, H.-C. zurLoye, T. Guidi, and D. T. Adroja, Phys. Rev. Lett. **112**, 117603 (2014).
[11] A. A. Aczel, D. E. Bugaris, L. Li, J.-Q. Yan, C. de la Cruz, H.-C. zurLoye, and S. E. Nagler, Phys. Rev. B **87**, 014435 (2013).
[12] K. Yamamura, M. Wakeshima, and Y. J. Hinatsu, Solid State Chem. **179**, 605 (2006).
[13] Y.-J. Song, K.-H. Ahn, and K.-W. Lee, and W. E. Pickett, Phys. Rev. B **90**, 245117 (2014).
[14] A. J. Steele, P. J. Baker, T. Lancaster, F. L. Pratt, I. Franke, S. Ghannadzadeh, P. A. Goddard, W. Hayes, D. Prabhakaran, and S. J. Blundell, Phys. Rev. B **84**, 144416 (2011).
[15] A. S. Erickson, S. Misra, G. J. Miller, R. R. Gupta, Z. Schlesinger, W. A. Harrison, J. M. Kim, and I. R. Fisher, Phys. Rev. Lett. **99**, 016404 (2007).
[16] K. E. Stitzer, M. D. Smith, and H.-C. Z. Loye, Solid State Sci. **4**, 311 (2002).
[17] C. M. Thompson *et al.*, J. Phys.: Condens. Matter **26**, 306003 (2014).
[18] E. Kermarrec, C. A. Marjerrison, C. M. Thompson, D. D. Maharaj, K. Levin, S. Kroeker, G. E. Granroth, R. Flacau, Z. Yamani, J. E. Greedan, and B. D. Gaulin, Phys. Rev. B **91**, 075133 (2015).
[19] W. R. Gemmill, M. D. Smith, R. Prozorov, and H.-C. zur Loye, Inorg. Chem. **44**, 2639 (2005).
[20] Y. Shi, Y. Guo, Y. Shirako, W. Yi, X. Wang, A. A. Belik, Y. Matsushita, H. L. Feng, Y. Tsujimoto, M. Arai, N. Wang, M. Akaogi, and K. Yamaura, J. Am. Chem. Soc. **135**, 16507 (2013).
[21] M-C. Jung, Y.-J. Song, K.-W. Lee, and W. E. Pickett, Phys. Rev. B **87**, 115119 (2013).
[22] K. W. Lee and W. E. Pickett, Europhys. Lett. **80**, 37008 (2007).
[23] T. Shirakawa, H. Watanabe, and S. Yunoki, J. Phys.: Conf. Ser. **400**, 032088 (2012).
[24] H. Zhang, K. Haule, and D. Vanderbilt, Phys. Rev. Lett. **111**, 246402 (2013).
[25] V. I. Anisimov, J. Zaanen, and O. K. Andersen, Phys. Rev. B **44**, 943 (1991).
[26] A. I. Liechtenstein, V. I. Anisimov, and J. Zaanen, Phys. Rev. B **52**, R5467(R) (1995).
[27] E. R. Ylvisaker, W. E. Pickett, and K. Koepernik, Phys. Rev. B **79**, 035103 (2009).
[28] H. J. Xiang and M.-H. Whangbo, Phys. Rev. B **75**, 052407 (2007).

[29] Y. Quan, V. Pardo, and W. E. Pickett, Phys. Rev. Lett. **109**, 216401 (2012).
[30] W. E. Pickett, Y. Quan, and V. Pardo, J. Phys.: Condens. Matter **26**, 274203 (2014).
[31] Y. Quan and W. E. Pickett, Phys. Rev. B **91**, 035121 (2015).
[32] E. Pavarini and I. I. Mazin, Phys. Rev. B **76**, 079901(E) (2007).
[33] P. Blaha, K. Schwarz, G. Madsen, D. Kvasicka, and J. Luitz, WIEN2K, An Augmented Plane Wave + Local Orbitals Program for Calculating Crystal Properties, Technical University of Vienna, Vienna, 2001. We have used version 12 of WIEN2K, because we have found that SOC with the hybrid functional does not always work correctly in version 13.
[34] F. Tran, P. Blaha, K. Schwarz, and P. Nov'ak, Phys. Rev. B **74**, 155108 (2006).
[35] P. Novák, J. Kuneš, L. Chaput, and W. E. Pickett, Phys. Status Solidi B **243**, 563 (2006).
[36] In the WIEN2K case.inorb file the flag HYBR is used for Os 5*d* orbitals, with a fraction of 0.25.
[37] J. P. Perdew, K. Burke, and M. Ernzerhof, Phys. Rev. Lett. **77**, 3865 (1996).
[38] A. H. MacDonald, W. E. Pickett, and D. D. Koelling, J. Phys. C **13**, 2675 (1980).
[39] R. Laskowski and P. Blaha, Phys. Rev. B **85**, 245117 (2012).
[40] R. Laskowski and P. Blaha, Phys. Rev. B **85**, 035132 (2012).
[41] R. Laskowski, P. Blaha, and F. Tran, Phys. Rev. B **87**, 195130 (2013).
[42] R. Laskowski and P. Blaha, Phys. Rev. B **89**, 014402 (2014).
[43] C. J. Pickard and F. Mauri, Phys. Rev. B **63**, 245101 (2001).
[44] A. Kokalj, J. Mol. Graphics Modell. **17**, 176 (1999); Comput. Mater. Sci. **28**, 155 (2003).
[45] S.-T. Pi, R. Nanguneri, and S. Savrasov, Phys. Rev. Lett. **112**, 077203 (2014).
[46] S.-T. Pi, R. Nanguneri, and S. Savrasov, Phys. Rev. B **90**, 045148 (2014).